Archive of SID

Transaction B: Mechanical Engineering
Vol. 17, No. 5, pp. 406–417
© Sharif University of Technology, October 2010

Research Note

SCIENTIA IRANICA

An Approach to the Design of Ducted Propeller

F. Çelik[1,*], M. Güner[1] and S. Ekinci[1]

Abstract. *This paper describes a design methodology for ducted propellers operating in a non-uniform wake field. An improved lifting line model is used to represent propeller blades where more realistic slipstream deformation behind the propeller is considered, while the duct and hub are modeled by ring vortex distributions. Duct and hub geometries are assumed to be known and their effects on the propeller are calculated during propeller design stage. At the same time, mutual interaction between duct/hub geometry and propeller is taken into consideration based on an iterative procedure. For numerical application of the present method, a design example is carried out and the effect of slipstream deformation is investigated in detail. Another application based on experimental work is also taken into account to present the accuracy of the calculated results by present method and Computational Fluid Dynamics (CFD) code. Finally, propulsive characteristics of ducted propellers obtained from present method are compared to those of CFD code and experimental results.*

Keywords: *Ducted propeller; Lifting line method; Surface vorticity method; CFD; Slipstream deformation.*

INTRODUCTION

Screw propellers are the most common form of marine propulsion device for the last 150 years. As they transform the power generated by main engine to the thrust force, inevitably some energy losses occur. Especially in case of heavily loading of propeller, the most important energy loss becomes in axial direction. The use of an accelerating type of duct (Kort Nozzle) around the propeller is an easy way of increasing propulsion efficiency by reducing axial losses. As ducted propellers supplying energy saving up to 20%, they are adopted into a range of marine vessels, such as commercial ships, tugboats, bulk carriers, submarines, trawlers etc.

The first studies related to ducted propellers were carried out by Stipa and Kort and developed by experimental works in 1930s [1]. They showed that application of duct increases propulsive efficiency for heavily loaded propellers. The first experimental design studies taken into account of interaction between duct and propeller were carried out systematically using Ka propeller series at Maritime Research Institute Netherlands (MARIN), and these studies were reported by van Manen and Oosterveld [1]. Sparenberg [2] showed that the duct did not contribute to propulsion efficiency for lightly loading case as representing the propeller by an actuator disc in a duct. Nevertheless interaction between duct and propeller was not taken into account sufficiently in any of these methods. In the later years, developments of computer technology allowed more complex models based on circulation theory, considering more precise duct-propeller interaction rather than basic propeller models.

One of the most significant studies for ducted propeller design was carried out by Ryan and Glover [3]. The propeller was modeled by lifting line method, and duct and hub by axisymmetric surface vorticity method. In this ducted propeller design procedure, lifting line method developed by Glover [4] was used, where it is allowed the slipstream deformation partially. In order to obtain the induction factors for an irregular helix, Glover suggests that the helix should be split up into a number of finite regular helical elements. The lengths of these elements should be small in areas where the pitch and diameter of the irregular helix changes most. Furthermore, their pitch and diameter should be equal to the arithmetic mean of the irregular element they represent.

1. *Department of Naval Architecture, Yildiz Technical University, 34349 Besiktas, Istanbul, Turkey.*
*. *Corresponding author. E-mail: fcelik@yildiz.edu.tr*

Received 22 December 2009; received in revised form 8 July 2010; accepted 10 August 2010

www.SID.ir

Archive of SID

Kinnas and Coney [5] presented a ducted propeller design method where duct was modeled by source/sink distributed over the panels forming duct surface and propeller was represented by lifting lines. Optimum loading distribution over lifting line was obtained by using a non linear numerical optimization technique. There have been a number of studies achieved for analysis problem of ducted propeller, where the propeller was represented by lifting line, lifting surface or surface panel methods, the duct was modeled by surface vorticity, surface panel or lifting surface methods [6-11]. Kim et al. [12] presented a CFD method based on solving RANS equations to investigate a ducted propeller system in terms of acoustic and cavitation. Gu and Kinnas [13] and Kinnas et al. [14] developed an analysis procedure using a vortex lattice and finite volume methods together for modeling flow around a ducted propeller. Hsiao and Chahine [15] presented a numerical analysis method, using Navier-Stokes calculations and bubble dynamic, to predict cavitation phenomena for the ducted propellers. In this area, some recent studies have been presented in [16-18].

In this study a ducted propeller design method is presented, where duct is modeled by surface vorticity method developed by Ryan and Glover [3] and propeller blades are represented by an improved lifting line theory [19]. In the present design method, the radially varying inflow velocity of ducted propeller and wake in the downstream of propeller are also included to the calculations. In addition, propeller design procedure allows the deformation of slipstream behind the propeller in terms of pitch and radius of vortex lines for all loading conditions. As the earlier lifting line models, there were a number of simplifying assumptions imposed due to limitation on computational resources. One of these assumptions is that the propeller is assumed to be moderately loaded and that the downstream variation in induced velocities and hence the resulting slipstream deformation could be neglected [20]. Duct/hub geometries are considered to be known and their effects on the propeller are taken into account during propeller design stage. The interaction between duct/hub geometry and propeller is taken into consideration based on an iterative manner. As the experimental results of a ducted propeller model are compared with those of present method and Computational Fluid Dynamics (CFD) code, validation of the methods is realized. Also, a design application of a ducted propeller for fishing vessel is implemented, and the effect of slipstream deformation, axial, tangential and radial velocity distributions in the downstream of the propeller, variation of hydrodynamic pitch angles of trailing vortex lines, and pressure distributions over duct and hub surfaces are investigated in detail. Radial distributions of bound circulations, lift coefficients and hydrodynamic pitch angles are obtained from present and classical methods, and the results are compared in figures. Finally, the propulsive characteristics of ducted propeller for fishing vessel derived from present method are compared with the results of classical and CFD methods.

PROPELLER DESIGN PROCEDURE

In this section, a brief overview of the theoretical background of an "Improved Lifting Line Procedure" developed by Güner [21], and Celik and Güner [19] is used for ducted propeller design. The procedure makes use of the assumption that the blades are to be replaced by lifting lines, with zero thickness and width, along which the bound circulation is distributed. The free vortex sheets shed from the lifting lines lie on a helical surface, the shape of which is a function of velocities induced in the slipstream by the propeller and the body wake velocities. The method considers that the propeller has zero skew and rake.

The aim of the design is to obtain a solution of the vortex model of the propeller and, in particular, the determination of the distribution of the bound circulation on the lifting line such that the propulsor absorbs a given power at a specified rate of rotation and propeller advance speed.

When the propeller operates in the proximity of the sea surface the necessary blade surface area, required to minimize the risk of cavitation can be determined using an appropriate cavitation criteria, such as that due to Burrill [22]. The distribution of this area on an appropriate blade outline gives the blade chord widths at the design radii. A simple beam theory of stressing calculation can be used to calculate the blade section thickness and drag coefficient can be determined as a function of the section thickness ratios. The wake-adaptation of the design (i.e. optimization with respect to the radial wake distribution in which the propeller is assumed to work) is then carried out using the improved lifting line procedure.

In this procedure, the design conditions have to be satisfied in such a way that required torque coefficient K_Q, given by:

$$K_Q = \frac{33.55 P_D}{\left[\frac{ND}{10}\right]^3 D^2}, \tag{1}$$

where, P_D is the delivered power in kW; N is the propeller rate of rotation in per minute and, D is the propeller diameter in meters.

Optimization of the design, i.e. the determination of the radial loading distribution corresponding to maximum efficiency, is achieved by introducing a minimum energy loss condition into the solution of the lifting line model. In this study, the condition derived

www.SID.ir

Archive of SID

by Burrill [23] is used in which the vortex sheets in the ultimate wake are assumed to have uniform pitch radially, i.e.:

$$x_i \pi \tan \varepsilon_i = \text{constant}, \tag{2}$$

where $x_i = r_i/R$ is the non-dimensional form of the ith section radius, R is the propeller radius and ε_i is the pitch angle of helical vortex sheets at infinity.

Based on the assumptions that the circulation of the lifting line, or bound circulation, is assumed to go continuously to zero at both the tip and the boss, the associated expression for the circulation can be defined by a Fourier sine series and written in non-dimensional form as follows:

$$G_i = \frac{\Gamma_i}{\pi D V_s} = \sum_{n=1}^{\infty} A_n \sin(n\phi_i), \tag{3}$$

where Γ_i is the bound circulation at x_i and A_n is the bound circulation coefficient whose value is to be determined.

The angular coordinate, ϕ_i, is defined in terms of the radial coordinate, x_i, as follows:

$$x_i = x_h + \left(\frac{1 - x_h}{2}\right)(1 - \cos\phi_i), \tag{4}$$

where x_h is the non-dimensional hub radius and ϕ_i varies from 0 at the hub to π at the tip.

The problem is now reduced to the determination of the unknown A_n's. Once these values are calculated, the axial, tangential and radial induced velocities at any point of the lifting line can be estimated and finally the hydrodynamic pitch angle, lift coefficient and torque and thrust coefficients can be calculated.

The solution of the lifting line design problem reduces to the determination of the values of the coefficients, A_n, such that the design conditions and a prescribed condition for minimum energy loss are satisfied. To effect the solution, the series is truncated to 9 terms and expressions for induced velocity components derived at 9 reference points along the lifting line in terms of A_n's and the induction factors. The induction factors depend only on the geometry of the slipstream and can be derived from the application of the Biot-Savart Law.

Total induced velocity of a point at radius x_i by helical lines starting at points x_k can be written in the axial, tangential and radial directions as follows:

$$u_{a,t,r} = \int_{x_h}^{xt} I_{a,t,r} \left(\frac{dG}{dx}\right)_k \frac{dx_k}{2(x_i - x_k)}. \tag{5}$$

$I_{a,t,r}$ is the Induction Factors in the axial, radial and tangential direction, respectively:

in the axial direction:

$$I_a = \sum_1^Z (x_i - x_k) \int_0^{\infty} \tan\beta_{kj} \frac{x_{kj}}{a^3} (x_{kj} - x_i \cos(\theta_{kj} + \phi_z)) d\theta, \tag{6}$$

in the tangential direction:

$$I_t = \sum_1^Z (x_i - x_k) \int_0^{\infty} \tan\beta_{kj} \frac{x_{kj}}{a^3} (x_i - x_{kj} \cos(\theta_{kj} + \phi_z) - y_{kj} \cot\beta_{kj} \sin(\theta_{kj} + \phi_z)) d\theta, \tag{7}$$

and in the radial direction:

$$I_r = \sum_1^Z (x_i - x_k) \int_0^{\infty} \tan\beta_{kj} \frac{x_{kj}}{a^3} (y_{kj} \cot\beta_{kj} \cos(\theta_{kj} + \phi_z) - x_{kj} \sin(\theta_{kj} + \phi_z)) d\theta. \tag{8}$$

In Equation 5, when x_i approaches x_k, the integrants tends to infinity. But this difficulty can be resolved by considering a narrow space on either side of the reference point within which the integrant assumes certain values as defined by Güner [21] in detail.

At a point x_{ij} a distance y_{ij} downstream from the lifting line, the slope of the vortex line is given by:

$$\tan\alpha_{ij} = \frac{U_{r_{ij}} + u_{r_{ij}}}{U_{a_{ij}} + u_{a_{ij}}}, \tag{9}$$

where $U_{a_{ij}}$ and $U_{r_{ij}}$ are the local wake velocities in the axial and radial directions and $u_{a_{ij}}$ and $u_{r_{ij}}$ are the propeller induced velocities in the axial and radial directions, respectively.

The radius of the vortex line can then be determined from the following equation:

$$x_{ij} = x_i + \int_0^{y_{ij}} \tan(\alpha_{ij}) d\alpha_i. \tag{10}$$

The hydrodynamic pitch angle of the trailing vortices in the slipstream becomes:

$$\beta_{ij} = \tan^{-1}\left[\frac{U_{a_{ij}} + u_{a_{ij}}}{\pi x_{ij} n D - u_{t_{ij}}}\right], \tag{11}$$

where n is the propeller rate of rotation per second and $u_{t_{ij}}$ is the propeller induced velocities in the tangential direction.

As can be seen from Equations 10 and 11, the deformed slipstream shape depends on the total velocity on the vortex lines. The total velocity can be defined as the sum of velocities induced at the point by the trailing vortices in the slipstream, bound vortices at

www.SID.ir

Archive of SID

the lifting line and the local wake velocities. As long as the total velocity at the point is calculated correctly, the true shape of the slipstream can be obtained.

In the present work, 21 control points are distributed axially along each of 12 lines placed at various radial locations. Of the radial control points, 11 are situated at the propeller design section radii and an extra point is placed below the propeller hub radius to allow the calculation of the wake velocities within the contracted propeller slipstream. The axial control points are placed at the following non-dimensional distances, Y/R, downstream of the propeller plane:

$$\frac{Y}{R} = 0.0, 0.06, 0.2, 0.4, 0.6, 0.8, 1.0, 1.2, 1.4, 1.6, 1.8,$$

$$2.0, 4.0, 6.0, 8.0, 10.0, 12.0, 14.0, 16.0, 18.0, 20.0.$$

In order to achieve convergence of the helical slipstream shape, the total velocities are calculated at each of the control points located on the reference vortex lines. Their location with respect to the lifting line is given as follows:

$$\theta = 0, \frac{\pi}{16}, \frac{\pi}{8}, \frac{\pi}{4}, \frac{3\pi}{8}, \frac{\pi}{2}, \frac{3\pi}{4}, \pi, \frac{5\pi}{4}, \frac{3\pi}{2}, \frac{7\pi}{4},$$

$$2\pi, 2.5\pi, 3\pi, 3.5\pi, 4\pi, 4.5\pi, 5\pi, 6\pi, 7\pi, 12\pi.$$

Hence, 231 control points are used for the representation of the slipstream. For the initial numerical calculation to define the trailing vortex shape, the local wake velocities only are used since the induced velocities are still unknown. Using this slipstream shape the bound circulation can be defined, and the means for the calculation of the induced velocities can be provided. Having calculated the induced velocities related to the previously established bound circulation, a new slipstream shape is obtained. According to the new deformed helical slipstream shape, the induction factors and the bound circulation are redefined and consequently the velocities induced at control points are recalculated. This procedure is carried out until a satisfactory result is obtained with the aim of modeling a final stable irregular helical slipstream shape. The design also satisfies the power absorption condition. This convergence can be achieved by 3 or 4 iterations. At least 3 iterations are essential to ensure the accuracy of the results.

In order to obtain the bound circulation, the integration of Equation 5 is carried out numerically such that for each of nine values of x_i, the nine term of equations for the induced velocity components are setup in terms of A_n's. By substituting this Equation into Burrill's condition, a system of nine simultaneous equations is formed as follows:

$$u_{ai} - u_{ti}\tan\varepsilon_i = \frac{1}{2}\left[\frac{x_i \pi \tan\varepsilon_i}{\frac{V_S}{nD}} - (1 - w_i)\right],$$

$$i = 1, 2, 3 \cdots, 9. \tag{12}$$

Solution of Equation 12 gives the circulation coefficients and hence the bound circulation.

Finally the propeller thrust and torque coefficients of each blade section are calculated, respectively, as below:

$$\left(\frac{K_T}{dx}\right)_i = \frac{\left(\frac{c.C_L}{D}\right)_i . \left[\frac{\pi x}{J} - u_{ti}\right]^2 . J^2 \left(1 - \frac{C_D}{C_L}.\tan\beta_i\right)}{4\cos\beta_i}, \tag{13}$$

$$\left(\frac{K_Q}{dx}\right)_i = \frac{x_i . \left(\frac{c.C_L}{D}\right)_i . [(1-w_i)+u_{ai}]^2 . J^2 \left(1 - \frac{C_D}{C_L}.\tan\beta_i\right)}{8\sin\beta_i}, \tag{14}$$

where:

$$\left(\frac{cC_L}{D}\right)_i = \frac{2\pi G_i \sin\beta_i}{(1 - w_i) + u_{ai}}. \tag{15}$$

The drag coefficient for each propeller section can be calculated in terms of propeller blade thickness and chord length as below:

$$C_D = 2\left(1 + 2\frac{t_i}{c_i}\right).\left[1.89 + 1.62\log\left(\frac{c_i}{30.10^{-6}}\right)\right]^{-2.5}. \tag{16}$$

DUCTED PROPELLER DESIGN PROCEDURE

In the present ducted propeller design method, the optimum circulation distribution of a propeller inside a duct is obtained, and the flow analysis is carried out for existing duct and hub. The propeller design and the flow analysis are performed separately, but flow interaction between each other is included to the computations as an iterative procedure.

For flow analysis of duct/hub, a surface vorticity method developed by Ryan and Glover [3] is used. In this method, duct and hub geometries are represented by continuously distributed ring vortices $\gamma(s)$ over surfaces of them. Besides, it is assumed that the inflow to duct/hub and their geometries are axisymmetric, and the fluid is inviscid. Strengths of ring vortices $\gamma(s)$ modeling duct and hub are determined in a manner of providing Dirichlet boundary condition, i.e. tangential velocity component of flow at any point over surfaces

www.SID.ir

Archive of SID

is required as zero. For this purpose, a linear equation system is obtained by forming boundary condition over whole surfaces. For any control point (s_m) taken over surfaces, the governing equation explaining Dirichlet boundary condition can be written as follows:

$$-\frac{1}{2}\gamma(s_m) + \int \gamma(s_n)K(s_m, s_n)ds_n + U_a.\cos\beta_m + U_r.\sin\beta_m = 0, \quad (17)$$

where m is the panel at which control point was located, n is the panel of ring vortex, γ is the unit vortex strength, U_a and U_r are axial and radial components of flow coming to control point, and β_m is the slope of the panel. $K(s_m, s_n)$ is a coupling coefficient which relates the induced velocity parallel to the surface at the point s_m due to a ring vortex of unit strength located at s_n. Induced velocities of ring vortices are calculated by means of Biot-Savart law [24].

If duct/hub geometries and the incoming flow are given, the strengths of ring vortices modeling duct and hub could be determined by numerically solving linear equation system such that the flow satisfies the Kutta condition at the trailing edge. It requires an assumption that the tangential velocity at the trailing edge must be smooth. This condition can be achieved such that the vortex strength and, therefore, the velocity on the upper and lower surfaces near the trailing edge are to be of the same magnitude. However, in order to achieve a smooth flow leaving the trailing edge, their directions must be opposite, i.e.:

$$\gamma(s_{te+1}) = -\gamma(s_{te}). \quad (18)$$

After the strength of vortices is determined, the pressure distribution on the duct and hub can be evaluated from Bernoulli's equation. In addition, the velocity induced by the duct and hub can be also predicted using vortices.

For ducted propeller design, an iterative procedure consisting four stages is applied:

- **First step**: The strengths of ring vortices modeling duct/hub geometries and the axial velocity components induced at propeller disc by those vortices are obtained. Then axial velocities induced by duct/hub are added to the wake varying radially at the propeller disc.
- **Second step**: The strengths of vortex lines are found in a way of satisfying "Minimum Energy Loss Condition".
- **Third step**: Propeller characteristics are calculated, and the axial and radial velocity components induced at control points of duct/hub surfaces by propeller vortex system are obtained. Induced velocities of propeller vortex system are calculated by means of Biot-Savart law.
- **Fourth step**: The strength of vortex elements modeling duct and hub are calculated.

The four steps expressed above are repeated until difference of consecutive two induced velocities of duct at propeller disc remains in an acceptable tolerance interval. Once the convergence is supplied, pressure distributions on duct/hub surfaces and performance coefficients are obtained. Then varying hydrodynamic pitch angles at all radii and optimum loading distribution of propeller could be achieved. Consequently, propeller characteristic coefficients are also calculated, and ducted propeller design is completed.

Besides the propeller design method presented above can be applied to design of ducted propellers, it is also capable of applying to propeller with stator or combined duct and pre or post stator systems.

DESIGN APPLICATION OF A DUCTED PROPELLER FOR FISHING VESSEL

In this section an application of the ducted propeller design procedure for a fishing vessel is considered. The propeller and duct data are given in Tables 1 and 2 respectively. The duct section is selected NSMB 19-A as shown in Figure 1. In order to demonstrate the effect of the slipstream contraction, a different ducted propeller design method (classical method) (where Lerb's lifting line method [20] is used for the propeller design, and duct and hub modeled by surface vorticity method) is also performed for case of non-deformed slipstream. Then, a CFD based on finite volume method is used for analysis of the ducted propeller.

Table 1. Propeller design input data.

Delivered power, P_D (kW)	530
Design speed, V_S (Knot)	10
Rate of rotation, RPM	317
Propeller diameter, D (m)	1.82
Number of blades, Z	4
Blade area ratio, (A_E/A_0)	0.7
Wake $(1-w)$	0.805
Advance ratio, J_A	0.431

Table 2. Duct data.

Section	NSMB Nozzle No 19-A
Length of duct, DC (m)	0.91 (0.5D)
Location of propeller	0.5 DC
Clearance between duct and Propeller (m)	0.002

www.SID.ir

Archive of SID

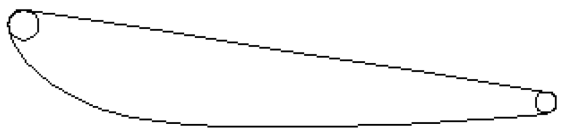

Figure 1. NSMB nozzle no 19-A section.

It is considered that the hub geometry consists of a cylinder and two semi spheres at its ends. The length of cylinder is equal to propeller diameter, D; the radius of semi spheres and cylinder is 0.2 R and the propeller is located at 0.75 length of cylinder.

Initially the axial flow velocity to the ducted propeller is assumed as uniform and remains constant along slipstream tube, but it is modified during iteration of the design procedure. The computation is performed for ducted propeller design based upon the procedure shown in Figure 2. Zero skew and rake of propeller are considered. During these computations, the slipstream shape of the propeller is converged in three iterations while meeting the required power absorption design condition. For the flow interaction among duct, hub and propeller, at least twenty five iterations are considered, but the convergence is obtained in ten iterations.

Figure 3 gives the radial variation of axial velocity at the propeller plane. As can be seen in this figure, high axial velocity due to the duct is occurred near tip region of propeller. In Figure 4 the slipstream contraction of propeller using the preset method is

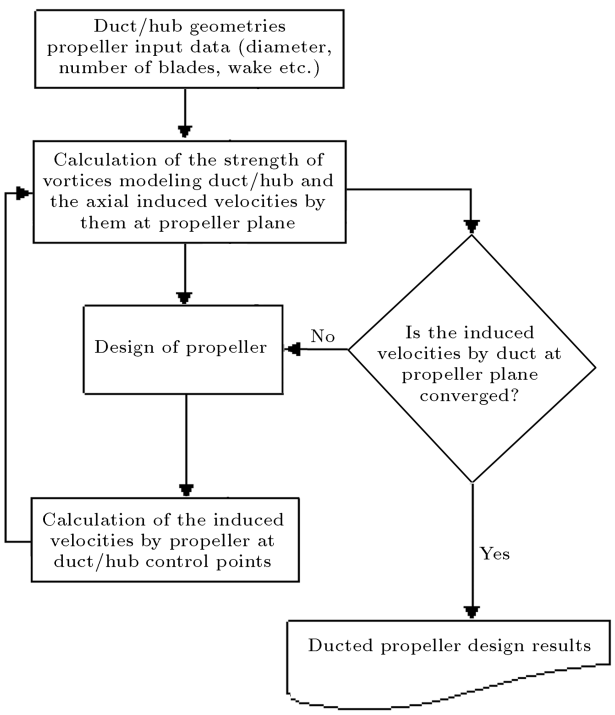

Figure 2. Flow diagram for ducted propeller design algorithm.

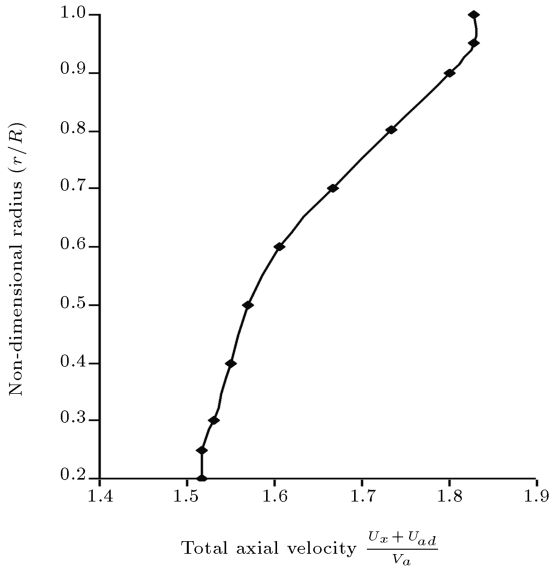

Figure 3. Radial variation of total axial velocity at propeller plane.

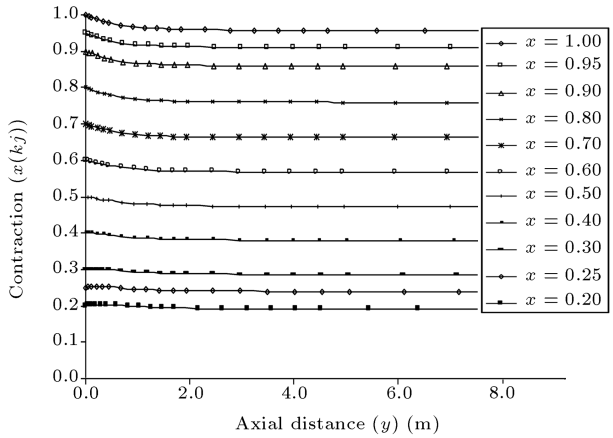

Figure 4. Slipstream contraction due to induced velocities.

shown. As seen in this figure, contraction ratio is approximately 0.95 at all radii. Near above hub radius in the downstream of the propeller, a small outward expansion is occurred instead of contraction due to the fact that positive radial induced velocities are occurred at this region.

Variation of the axial, tangential and radial induced velocities and hydrodynamic pitch angles of trailing vortex lines computed by the present method behind propeller are shown in Figures 5 to 8, respectively.

Figures 9 to 11 presents the radial distribution of bound circulation, lift coefficient and hydrodynamic pitch angle of the propeller blade computed by the present method in comparison with those by the method using Lerbs' lifting line (classical lifting line) method. Figures 9 to 11 suggest that there is not much

www.SID.ir

Archive of SID

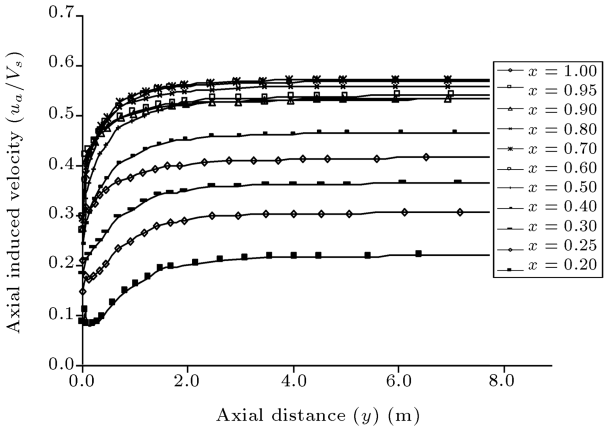

Figure 5. Variation of axial induced velocity in the downstream of propeller.

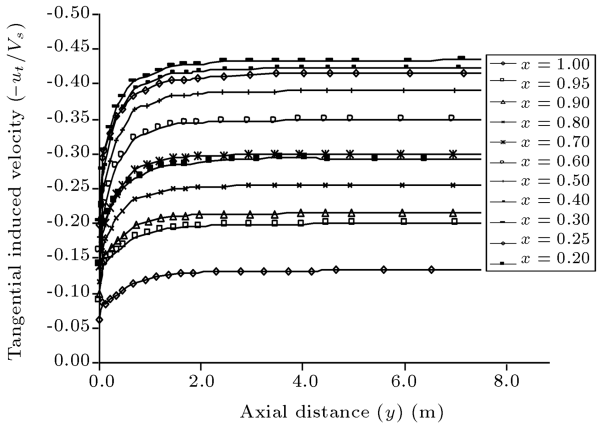

Figure 6. Variation of tangential induced velocity in the downstream of propeller.

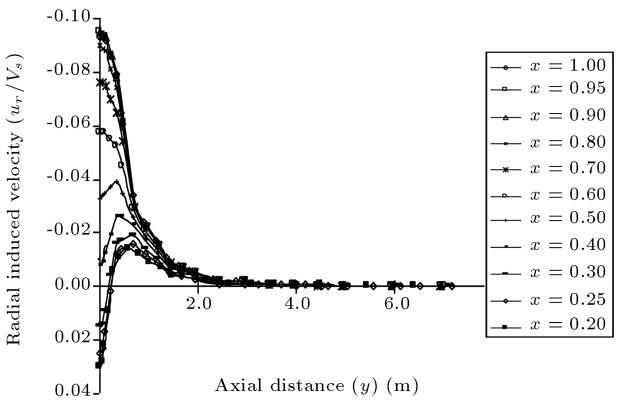

Figure 7. Variation of radial induced velocity in the downstream of propeller.

of a difference between the results obtained from both methods.

The slipstream shape behind one propeller blade obtained from the present method is found in Figure 12. As can be seen, far downstream of propeller has higher pitch with contracted radius.

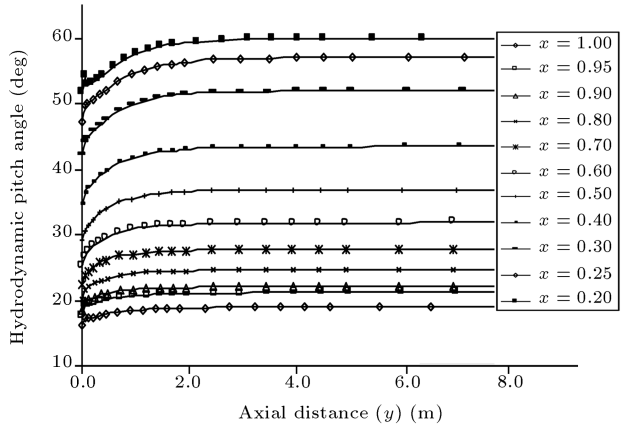

Figure 8. Variation of hydrodynamic pitch angle of trailing vortex lines in the downstream of propeller.

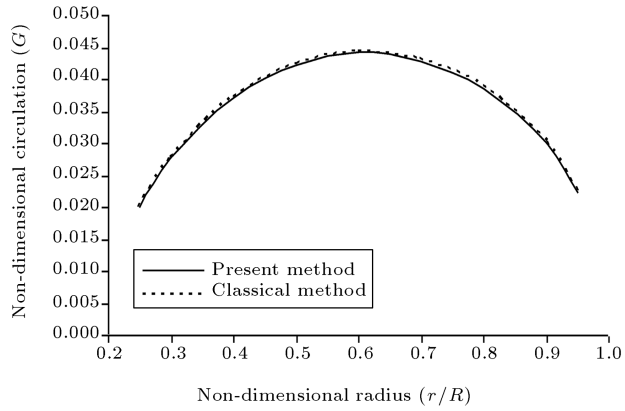

Figure 9. Radial distributions of bound circulation in non-dimensional form.

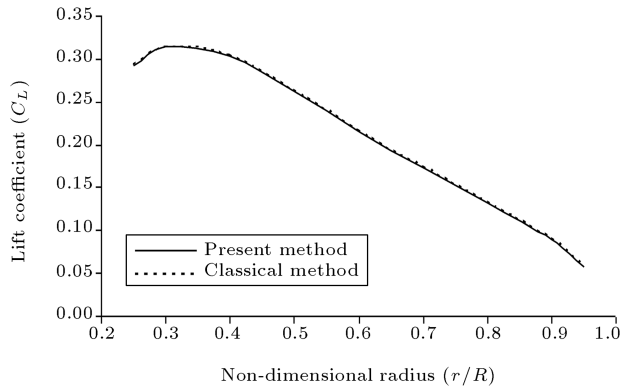

Figure 10. Lift coefficient of blade sections.

In Figures 13 and 14, pressure distributions over duct and hub surfaces from the present method are shown.

CFD Analysis

In CFD analysis of the ducted propeller, the solution is carried out by solving Reynolds Averaged Navier-

www.SID.ir

Archive of SID

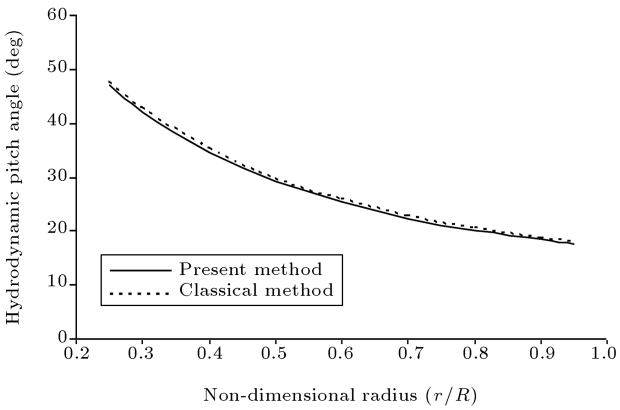

Figure 11. Radial hydrodynamic pitch angle distributions.

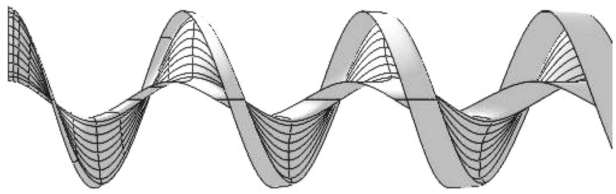

Figure 12. The slipstream of the propeller blade.

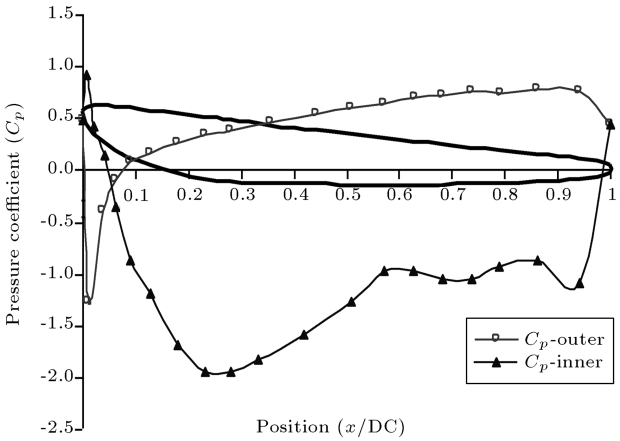

Figure 13. Pressure distributions over duct surface.

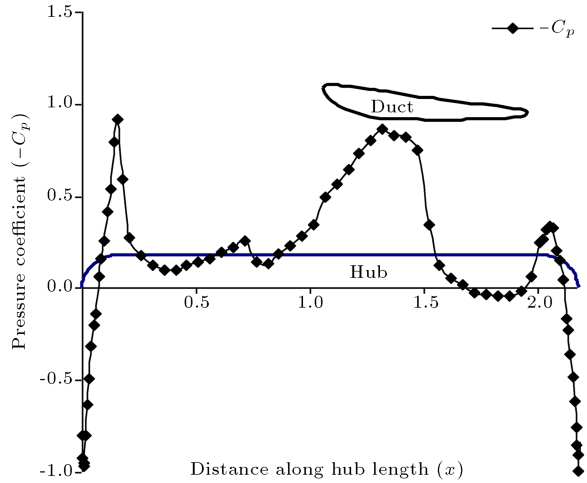

Figure 14. Pressure distribution over hub surface.

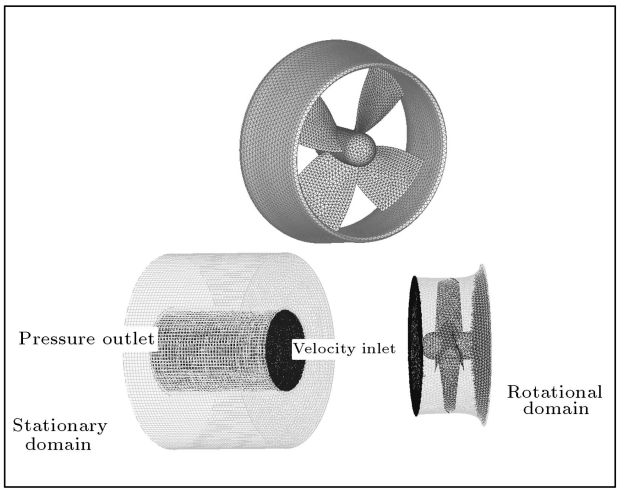

Figure 15. Arrangement of grid around ducted propeller.

Stokes (RANS) equations. As a RANS solver, a commercial CFD code Fluent 6.2.16 is used [25]. Detailed descriptions of the numerical method can be found in the User's Guide of this code.

Geometry and arrangement of grid around ducted propeller for fishing vessel shown in Figure 15 is modeled in Rhino CAD program and meshed using FLUENT pre-processor GAMBIT. The blade section geometry of the propeller is generated using NACA66 thickness with $a = 0.8$ mean line distributions for all radii. The computational domain is split into three parts: two cylindrical stationary parts and a moving part which is surrounded by inner surface of duct that rotates with the propeller. First, the blade and duct surfaces are meshed with smaller triangles. Then other surfaces which belong to moving and smaller cylindrical parts are meshed with larger triangles and these domains are filled with tetrahedral cells. Finally, a simple cylindrical mesh is generated for outer stationary block. On the outer boundary, the slip wall condition is imposed; on the blade, duct and hub surfaces, the no slip wall condition is imposed. The numbers of cells in this mesh are about 1,000,000.

The $k - \varepsilon$ (standard) is chosen as the turbulence model [26]. For solver, segregated, implicit and steady options are selected. In FLUENT, the governing equations are discretized using a second-order upwind interpolation scheme, and the discretized equations are solved using SIMPLE algorithm. Typical relaxation factors are chosen as 0.3, 0.7, 0.8 and 0.8 for pressure, momentum, turbulence kinetic energy and turbulence dissipation rate respectively. For both energy and turbulent viscosity, the relaxation factor is selected as 1. The solution is assumed converged when the continuity residual is lower than 10^{-5} and velocity

www.SID.ir

Archive of SID

Table 3. Comparison of the performance coefficients.

	Present Method	Classical Method	CFD
K_Q	0.0280	0.0284	0.0260
K_{TP}	0.1629	0.1634	0.1564
K_{TD}	0.0355	0.0350	0.0521
K_{TT}	0.1984	0.1984	0.2085
η	0.6044	0.5945	0.6832

residuals are lower than 10^{-6}. These residuals are reached at almost 2000 iterations.

In Table 3, the propulsion characteristics of the ducted propeller computed by present method are in comparison with those by the classical method using non-deformed lifting line and CFD code. As seen in this table, the present method gives a higher efficiency in comparison to classical methods, but difference is slight. So the realistic representation of the slipstream shape gives a higher efficiency in comparison to classical method for this application. However, CFD method gives a little higher efficiency.

Experimental Verification of the Theoretical and CFD Methods

Besides the application is presented above, here another application is taken into account in order to investigate the reliability of the present design and CFD analysis methods. For this purpose, a model propeller and duct geometries, whose experiments were carried out in the Emerson Cavitation Tunnel, are used. Main particulars of the model propeller and duct are given in Table 4 and complete results of the model test may be found in [27].

Design of the model ducted propeller, using present method, is carried out in the same manner as the first application and similar section shapes and hub geometry are used. The CAD modeling of the model ducted propeller geometry shown in Figure 16 and CFD analysis is also performed as stated before. But unsteady flow simulation for ducted propeller is carried out using moving mesh technique implemented in CFD code. At the velocity inlet boundary, the non-uniform inflow condition is imposed through the Boundary Profile (BP) feature of the code. The nominal wake distribution, Figure 17, is included to a BP file at 120 points.

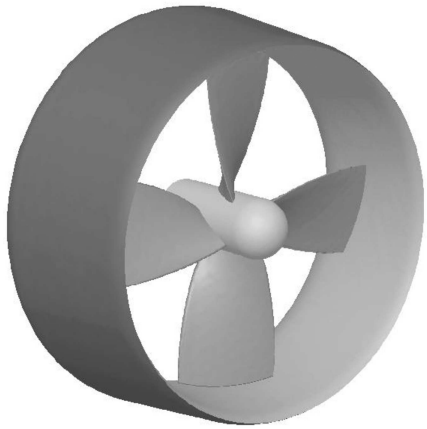

Figure 16. 3D CAD drawing of the model ducted propeller.

The results of the performance coefficients obtained from experiment, present design method and CFD code are given in Table 5.

As can be seen in Table 5, the present method and CFD results show a reasonably accurate prediction for ducted propeller performance.

CONCLUSIONS

The classical ducted propeller design methods using conventional lifting line theory for propeller representation assumes that the resulting slipstream shape is reg-

Table 4. Main particulars of the model propeller and duct.

Delivered power, P_D (kW)	4.518
Design speed, V_s (m/s)	3.048
Rate of rotation, RPS	27.71
Propeller diameter, D (m)	0.250
Number of blades, Z	4
Blade area ratio, (A_E/A_0)	0.55
Advance coefficient, J_A	0.433
Duct section	NSMB nozzle no 19-A
Length of duct, DC (m)	0.125 (0.5 D)
Location of propeller	0.5 DC
Clearance between duct and propeller (m)	0.002

www.SID.ir

Archive of SID

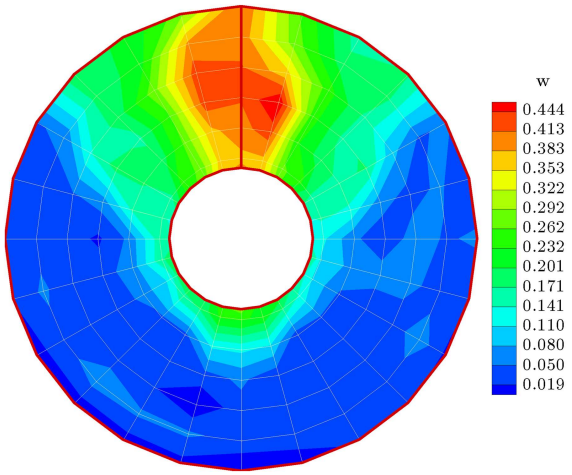

Figure 17. Nominal wake distribution of the model ducted propeller from experiment.

Table 5. Comparison of the performance coefficients.

	Present Method	CFD	Experiment
K_Q	0.0344	0.034	0.032
K_{TP}	0.185	0.205	0.180
K_{TD}	0.0413	0.032	0.040
K_{TT}	0.2263	0.237	0.220
η	0.454	0.486	0.474

ular, so it is considered that trailing vortex lines have constant radius and pitch angle. Especially in cases of heavily loading, this representation is insufficient. In this study an improved lifting line representation of propeller has been combined with surface vorticity method representation of duct and hub geometries. So a realistic approach has been developed in order to perform a design of ducted propeller operating in a non uniform inflow field to overcome disadvantage of the classical methods. The present method allows finding optimum propeller load distribution more accurately, and more realistic hydrodynamic characteristics and pitch distribution of propeller can be calculated. In addition realistic representation of the slipstream shape gives a higher efficiency in comparison to the classical methods. Present ducted propeller design method is also capable of applying to multiple stage propulsors such as combined duct and pre or post stator systems.

In this study, the present method has been applied to a design of ducted propeller for a fishing vessel. The ducted propeller performance characteristics obtained from present method is compared to those of a classical ducted propeller design method and a CFD method, and it is found that the results are not much of a difference. Another application is also carried out for validation of the present method and CFD code. It is also found that the results from present method and CFD code showed reasonable agreement with those of the experimental method.

NOMENCLATURE

A_n	Fourier terms of bound circulation
c	propeller blade section chord length
C_D	propeller blade section drag coefficient
C_L	propeller blade section lift coefficient
D	propeller diameter
ds	length of vortex element
G	non-dimensional bound circulation
i	subscript for propeller blade section number
j	subscript of control point along the slipstream
J	advance Coefficient
$I_{a,t,r}$	induction factors in the axial, tangential and radial directions
K_Q	torque coefficient
K_T	thrust coefficient
N	propeller rate of rotation per minute
P_D	delivered power
P	pitch
R	propeller radius
r	radius of reference point
t	thickness
$u_{a,t,r}$	induced velocities in the axial, tangential and radial directions
$U_{a,r}$	local wake velocities in the axial and radial directions
V_s	ship speed
w	Taylor wake fraction
x	non-dimensional radius
y/R	non-dimensional distances downstream of the propeller plane
x_h	non-dimensional hub radius
x_t	non-dimensional blade tip radius
Z	number of propeller blade
α	slope of vortex line
β_i	hydrodynamic pitch angle
δ	inverse of advance ratio
ε	hydrodynamic pitch angle at far downstream
η	efficiency

www.SID.ir

Archive of SID

Γ	bound circulation
ϕ	angular coordinate
θ	angle of rotation of blade from top dead centre

REFERENCES

1. Van Manen, J.D., Oosterveld, M.W.C. "Analysis of ducted propeller design", *Trans. SNAME*, **74**, pp. 522-561 (1966).
2. Sparenberg, J.A. "On optimum propellers with a duct of finite length", *Journal of Ship Research*, **35**(2), pp. 115-161 (1969).
3. Ryan, P.J. and Glover, E.J. "A ducted propeller design method: a new approach using surface vorticity distribution techniques and lifting line theory", *Trans. RINA*, **114**, pp. 545-563 (1972).
4. Glover, E.J. "Slipstream deformation and its influence on marine propeller design", PhD Thesis, University of Newcastle upon Tyne (1970).
5. Kinnas, S.A. and Coney, W.B. "On the optimum ducted propeller loading", *Proc. Propellers/Shafting'88 Symposium, SNAME*, pp 1.1-1.13, Virginia, USA (1988).
6. Falcao de Campos, JAC. "On the calculation of ducted propeller performance in axisymmetric flows", Technical Report 696, Netherlands Ship Model Basin, Wageningen, The Netherlands (1983).
7. Kerwin, J.E., Kinnas, S.A., Lee, J.T. et al. "A surface panel method for the hydrodynamic analysis of ducted propellers", *Trans. SNAME*, **95**, pp. 93-122 (1987).
8. Glover, E.J. and Szantyr, J. "The analysis of unsteady cavitation and hull surface pressures for ducted propellers", *Trans. RINA*, **132**, pp. 65-78 (1989).
9. Kinnas, S.A., Hsin, C.Y. and Kenan, D."A potential based panel method for the unsteady flow around open and ducted propellers", *Proc. Eighteenth Symposium on Naval Hydrodynamics*, pp. 667-684 (1991).
10. Kinnas, S.A and Coney, W.B. "The generalized image model - An application to the design of ducted propellers", *Journal of Ship Research*, **36**(3), 197-209 (1992).
11. Szantyr, J. "A surface panel method for analysis of open and ducted propellers", *Proc. Hydronav'97 Conference*, pp. 353-364, Wroclaw, Poland (1997).
12. Kim, J., Paterson, E. and Stern, F. "Verification & validation and sub-visual cavitation and acoustic modeling for ducted marine propulsor", *The 8th International Conference on Numerical Ship Hydrodynamics*, Busan, Korea (Sept. 22-25, 2003).
13. Gu, H. and Kinnas, S.A. "Modeling of contra-rotating and ducted propellers via coupling of a vortex-lattice with a finite volume method", *Propellers/Shafting 2003 Symposium, SNAME*, Virginia Beach, VA (Sept. 17-18, 2003).
14. Kinnas, S.A., Lee, H. and Gu, H. et al. "Prediction of performance of ducted and podded propellers", *25th Symposium on Naval Hydrodynamics*, St. John's, Newfoundland and Labrador, Canada (Aug. 8-13, 2004).
15. Hsiao, C.T. and Chahine, G.L. "Numerical study of cavitation inception due to vortex/vortex interaction in a ducted propulsor", *25th Symposium on Naval Hydrodynamics*, St. John's, Newfoundland and Labrador, Canada (Aug. 8-13, 2004).
16. Celik, F. "A numerical study for effectiveness of a wake equalizing duct", *Ocean Engineering*, **34**(16), pp. 2138-2145 (2007).
17. Phillips, A.B., Turnock, S.R. and Furlong, M. "Evaluation of manoeuvring coefficients of a self-propelled ship using a blade element momentum propeller model coupled to a Reynolds averaged Navier Stokes flow solver", *Ocean Engineering*, **36**(15-16), pp. 1217-1225 (2009).
18. Liu, P., Islam, M. and Veitch, B. "Unsteady hydromechanics of a steering podded propeller unit", *Ocean Engineering*, **36**(12-13), pp. 1003-1014 (2009).
19. Celik, F. and Güner, M. "An improved lifting line model for the design of marine propellers", *SNAME News and Marine Technology*, **43**(2), pp. 100-113 (2006).
20. Lerbs, H.W. "Moderately loaded propellers with a finite numbers of blades and an arbitrary distribution of circulation", *Trans SNAME*, **60**, pp. 73-117 (1952).
21. Güner, M. "A rational approach to the design of propulsors behind axisymmetric bodies", PhD Thesis, University of Newcastle upon Tyne, UK (1994).
22. Burrill, LC. "Calculation of marine propeller performance characteristics", *Trans N.E.C.I.E.S.*, **60** (1943-44).
23. Burrill, LC. "The optimum diameter of marine propellers", *Trans N.E.C.I.E.S.*, **72** (1955-56).
24. Lewis, R.I., *Vortex Element Methods for Fluid Dynamic Analysis of Engineering Systems*, Cambridge University Press, Cambridge, England (1991).
25. Fluent 6.2.16 User's Guide Fluent Inc (2004).
26. Launder, B.E. and Spalding, D.B., *Lectures in Mathematical Models of Turbulence*, Academic Press, London, England (1972).
27. Szantyr, J. "Results of experimental verification of the program for analysis of ducted propellers in the non-uniform inflow field", Emerson Cavitation Tunnel Report No.4/88, University of Newcastle upon Tyne (1988).

BIOGRAPHIES

Fahri Çelik was born in Isparta, Turkey in 1973. He received his B.S. in Naval Architecture and Marine Engineering from Istanbul Technical University in 1994 and a M.S. and a Ph.D. in the same course from Yildiz Technical University in 1997 and 2005, respectively. His research interests include: Marine Propellers, Ship

www.SID.ir

Archive of SID

Resistance and Propulsion, CFD and Unconventional Propulsion Systems.

Mesut Güner was born in Malatya, Turkey in 1967. He received his B.S. degree in Naval Architecture and Marine Engineering from Istanbul Technical University in 1988 and his M.S. and Ph.D. degrees in Marine Technology from Newcastle University, England in 1990 and 1994, respectively. His research interests include: Design and Analysis in Marine Propellers and Propulsors, Ship Resistance, Underwater Acoustics, Propeller/Hull Interaction and CFD.

Serkan Ekinci was born in Istanbul, Turkey in 1977. He received his BS, MS and PhD degrees in Naval Architecture and Marine Engineering from Yıldız Technical University in 1998, 2000 and 2007, respectively. His research interests include: Marine Propellers, Ship Resistance and Propulsion and Propeller Cavitation.

www.SID.ir